Characteristics of an Electrodynamic Wheel Using a 2-D Steady-State Model

Jonathan Bird and Thomas A. Lipo, *Life Fellow, IEEE*

University of Wisconsin-Madison, Madison, WI 53706 USA

The mechanical rotation of a radially positioned permanent-magnet Halbach array above a conducting, nonmagnetic track induces eddy currents in the track that can inductively create suspension and propulsion forces simultaneously. The parameters that affect the performance of this electrodynamic wheel are studied using a 2-D steady-state finite-element method. Tradeoffs between the lift and thrust force performance are investigated and methods to improve the thrust efficiency are proposed.

Index Terms—**Eddy currents, electromagnetic analysis, finite-element methods, Halbach array, maglev.**

I. Introduction

THE use of a single-sided linear induction motor (SLIM) with a track constructed of aluminum and back iron held early promise as a means of providing propulsion for high-speed ground transportation applications [1]–[14] and a high-speed way-side power collection method was developed in the USA [15]. But for high-speed operation, the SLIM suffers from a low power factor and it must be designed to be very long in order to counteract the end-effects [2], [3]. Typically a secondary electromagnetic attractive suspension system is used to provide the lift and guidance forces; however, using such a system increases costs and creates drag losses [16]–[19]. A more elegant and substantially lower cost method is to only use aluminum on the track. With no back iron, the induced eddy currents enable the SLIM to also create the suspension and guidance forces inductively using a flat guideway. This "electromagnetic river" concept was first proposed by Eastham and Laithwaite [20]; however, it has a very poor power factor [21], [22], and the lift-to-weight ratio is low, thus its practical implementation has never been realized.

If radial or axially positioned magnets are mechanically rotated above a conductive, nonmagnetic guideway such as aluminum [23]–[34] then the induced eddy currents can create the lift and thrust forces without the low power factor, and potentially create a high lift-to-weight ratio. An illustration of the radial magnet configuration is shown in Fig. 1. With this method, the drag force that is created by typical translational electrodynamic suspension is used to create the thrust [32], [33]. Although increased losses result from the mechanical rotation, only one mechanism is needed to create all the forces, thus reducing the overall losses compared to other maglev systems. The use of only aluminum sheets for the track could potentially make the track costs comparable to high-speed rail. In this paper, the parameters that affect the performance of an electrodynamic wheel (EDW) will be investigated using the 2-D steady-state current-sheet model presented in [34]. The primary aim is to determine whether high lift and thrust forces can be created while operating at high efficiency.

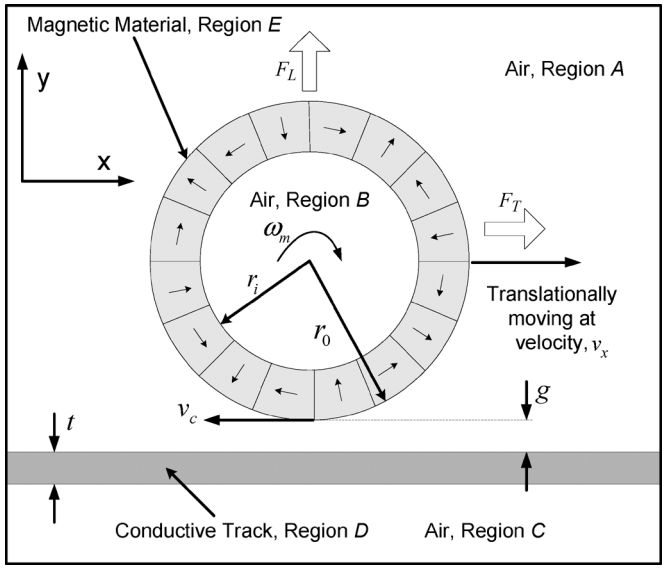

Fig. 1. An electrodynamic wheel translationally moving and rotating above a conductive, nonmagnetic track.

Modeling the steady-state forces using only a 2-D model neglects the effect of the field reduction along the z-axis and it does not account for the finite width of the guideway [35]. Consequently, it cannot account for the lateral (z-axis) force or the effect of the z-axis flux density, B_z, on the lift and thrust force. The exclusion of the third dimension also prevents any assessment of stability. However, despite these shortcomings the use of the 2-D steady-state model enables many salient features of the EDW to be initially assessed and these general characteristics, particularly thrust efficiency, should not be significantly affected by the third dimension.

A 3-D model of the EDW, track topologies that create lateral guidance force, and experimental results are presented in companion papers.

II. Optimal Halbach Rotor Magnet Thickness

The electrodynamic wheel could potentially use superconducting or rare-earth magnets to create the forces. However, this

Digital Object Identifier 10.1109/TMAG.2007.900572

Color versions of one or more of the figures in this paper are available online at http://ieeexplore.ieee.org.

analysis will focus on the use of rare-earth magnets with a Halbach array [36]–[38].

Previously, Davey proposed that for any inductive levitation device the highest lift-to-weight ratio, L_W, defined as

$$L_W = \frac{F_L}{mg} \tag{1}$$

can be obtained by minimizing the performance index: [39]

$$f_1(m, \Phi) = \frac{m}{\Phi^2} \quad [\mathrm{kgWb}^{-2}] \tag{2}$$

where

Φ	flux created by the magnet [Wb];
m	magnet mass [kg];
F_L	lift force [N];
g	gravitational acceleration, 9.81 ms^{-2}.

The use of (2) is reasonable if the magnet poles are repeating and have a uniform air-gap since only one magnet pole needs to be considered. However, since the Halbach rotor's air-gap above a flat track is not uniform the field contribution of each pole is not the same. Therefore, in order to determine the optimal lift-to-weight ratio for a full rotor, it is proposed that the absolute value of the magnetic vector potential, A_z, needs to be used when computing the "flux," such that

$$\Phi = \int_{\Gamma} |A_z| dl \quad [\mathrm{Wb}]. \tag{3}$$

The integration path, Γ, was chosen to span the width of the rotor along the top surface of the track. Using the absolute value of the vector potential incorporates both the positive and negative fields, preventing them from being cancelled out, since otherwise the net flux could be zero over the track surface. The rotor magnet mass will be

$$m = \pi \left(r_o^2 - r_i^2\right) \rho . w \quad [\mathrm{kg}] \tag{4}$$

where

r_o	rotor outer radius [m];
r_i	rotor inner radius [m];
ρ	magnet density [kgm^{-3}];
w	rotor width [m].

If the rotor radius ratio is defined as

$$Rr = \frac{r_i}{r_o} \tag{5}$$

then by substituting (3) and (4) into (2) and minimizing the radius ratio, for a given number of poles, the highest lift-to-weight ratio can be obtained.

As an example, (2) was evaluated for a range of inner radius values for the 4 pole-pair Halbach rotor shown in Fig. 1, with an outer radius fixed at 0.23 m. Finite-element analysis (FEA) was used to evaluate (3). The resulting values for the performance index are shown in Fig. 2. The optimal radius ratio for the 4 pole-pairs is seen to be $Rr = 0.68$, i.e., $r_i = 0.68 r_o$. In order to confirm that 0.68 gives the highest lift-to-weight ratio, the lift force was calculated for a range of radius ratios using the steady-state current sheet model [34] with the known rotor magnetic vector potential value. The parameters used are shown in Table I. Fig. 3 illustrates the results, and clearly shows that the peak lift-to-weight ratio indeed occurs when the radius ratio is 0.68.

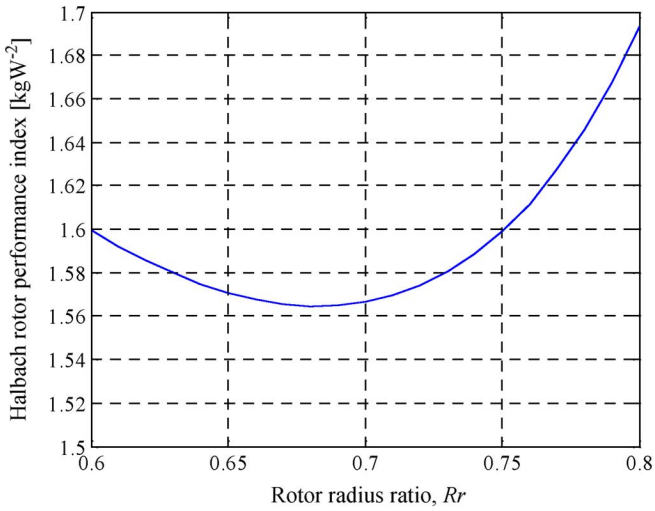

Fig. 2. Four pole-pair Halbach rotor performance measure for an outer radius, r_o, of 0.23 m.

TABLE I
SIMULATION PARAMETERS

Translational velocity, v_x	80 ms^{-1}
Slip speed, s	30 ms^{-1}
Outer radius, r_o	0.23 m
Inner radius, r_i	varied
Pole pairs, P	4
Track Thickness, t	10 mm
Magnet width, w	0.15 m
Air gap, g	10 mm
Track Conductivity, σ	$3.5\times10^7 \mathrm{Sm}^{-1}$
Magnet Residual magnetization, B_r	1.41 T
Magnet Permeability, μ_r	1.08

Interestingly, it was discovered that the optimal radius ratio, for each pole-pair is independent of the actual outer radius value. The optimal radius ratio calculated using this method for 2 to 7 pole-pairs is summarized in Fig 4.

III. Example of the Lift and Thrust Force Profile

The thrust force is created when the circumferential velocity, ν_c, of the EDW becomes somewhat greater than the translational velocity, ν_x. Thus, a slip speed s is always present, and is defined as

$$s = v_c - v_x \quad [\mathrm{ms}^{-1}]. \tag{6}$$

The circumferential velocity is defined as

$$v_c = \omega_m r_o \quad [\mathrm{ms}^{-1}] \tag{7}$$

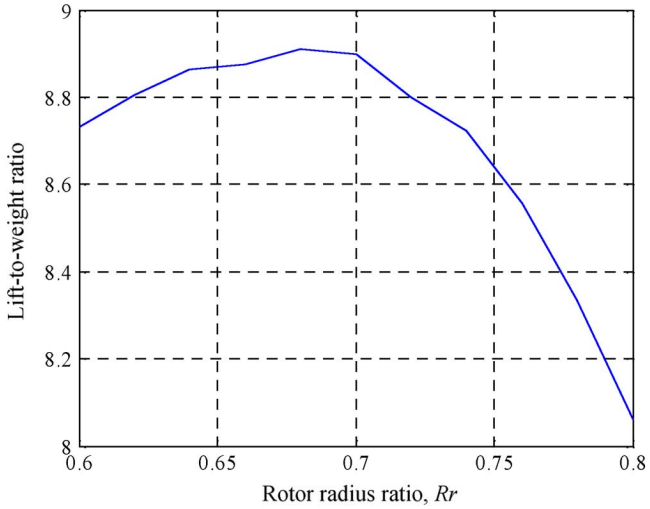

Fig. 3. Confirming the optimal lift-to-weight ratio for 4 pole-pair rotor using a the steady-state current sheet model.

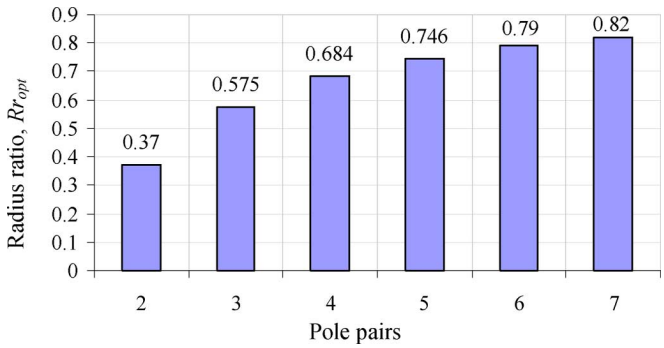

Fig. 4. Optimal radius ratio versus pole pairs.

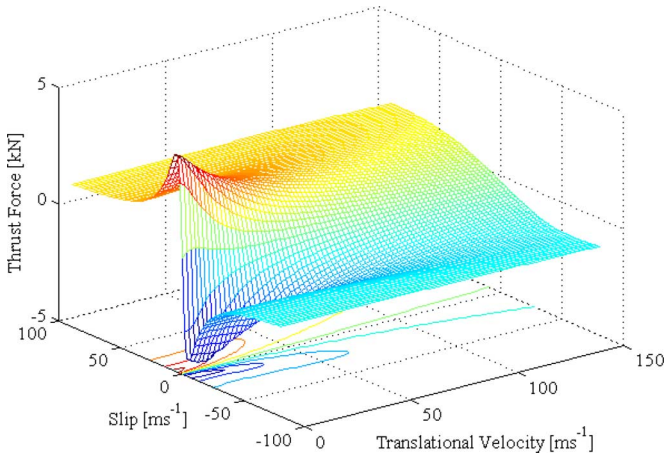

Fig. 5. Thrust force versus slip speed for a range of translational velocities.

$$= \frac{\omega_e r_o}{P} \tag{8}$$

where

ω_m	mechanical angular velocity;
ω_e	electrical angular frequency;
P	number of pole pairs.

A typical example of how the lift and thrust forces are affected by the slip speed and translational velocity is shown in Figs. 5 and 6. The 2-D steady-state current sheet model was used to calculate the results [34] and the parameters used are shown in Table II. Fig. 5 shows that in order to attain sufficient thrust the slip speed must be increased at higher translational velocities, like with the SLIM. Fig. 6 shows that the lift force becomes increasingly independent of slip speed as the translational velocity increases.

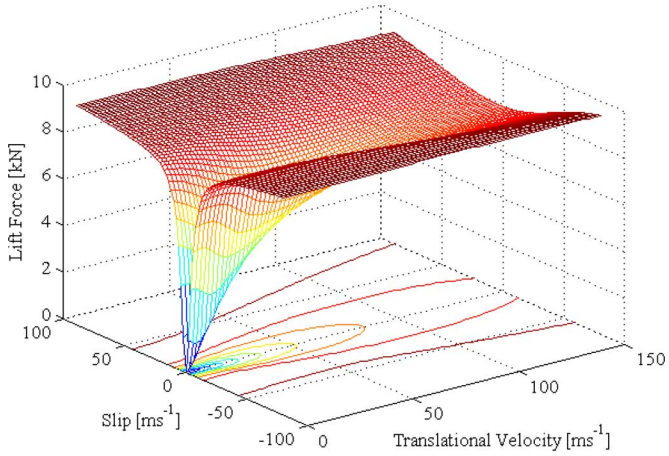

Fig. 6. Lift force versus slip speed for a range of translational velocities.

TABLE II
SIMULATION PARAMETERS

Translational velocity, v_x	varied
Slip speed, s	varied
Outer radius, r_o	0.23m
Track conductivity, σ	$3.5\times10^7 \mathrm{Sm}^{-1}$
Track thickness, t	10mm
Magnet width, w	0.2m
Air gap, g	10mm
Pole Pairs, P	6

Although the slip speed significantly influences the forces, it was determined that the general relationship between the parameters often scaled almost equally with slip speed and since two-dimensional plots more clearly show relationships wherever possible only one slip value has been used.

IV. PARAMETER ANALYSIS

This section summarizes the results from studying how various parameters affect the performance of an electrodynamic wheel, such as the number of pole-pairs, the outer radius, track thickness, and track conductivity. The radius ratio that gives the highest lift-to-weight is always used. In order to assess the performance, the following additional metrics were defined:

Thrust efficiency, η: [5], [23]

$$\eta = \frac{F_T v_x}{F_T v_x + P_{\mathrm{Loss}}} \tag{9}$$

$$= \frac{F_T v_x}{T \omega_m} \tag{10}$$

The lift mass, m_L, as:

$$m_L = \frac{F_L}{g} \quad [\mathrm{kg}] \tag{11}$$

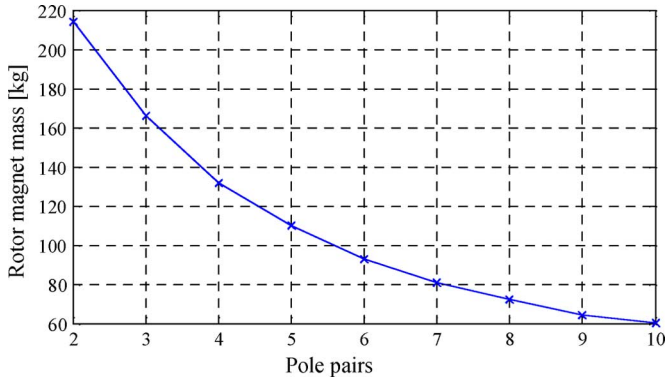

Fig. 7. Rotor magnet mass versus pole-pairs.

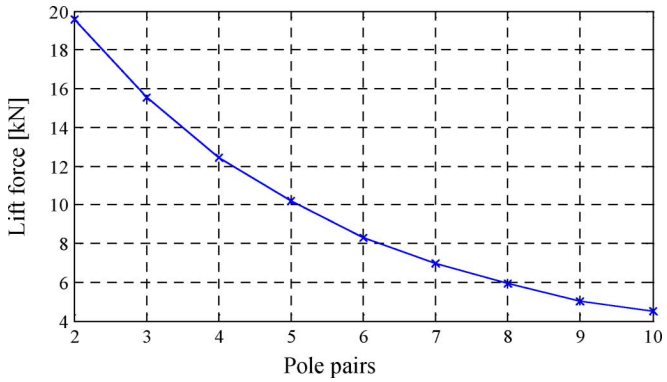

Fig. 8. Lift force versus pole-pairs.

Watts-per-kilogram, W_{pKg} as:

$$W_{pKg} = \frac{P_{\text{Loss}}}{m_L} \quad [\text{W/kg}] \tag{12}$$

and lift-to-thrust ratio, L_T:

$$L_T = \frac{F_L}{F_T}$$

where

F_T	thrust force;
T	mechanical torque;
P_{Loss}	eddy current power loss within the track.

A. Pole Pairs

Figs. 7–13 show how the pole-pairs influence the performance metrics, such as the magnet mass, lift force, thrust force, lift-to-weight ratio, track power, watts-per-kilogram for lift, lift-to-thrust ratio, and thrust efficiency. The parameters used for the pole-pair analysis are shown in Table III.

Fig. 7 shows that, for a given outer radius, the magnet mass decreases with an increase in pole-pairs. This is simply because the optimal radius ratio, Rr_{opt}, increases with the number of pole-pairs. The lift force, shown in Fig. 8, decreases with an increasing number of pole-pairs because the flux density over the track surface decreases. The thrust force, shown in Fig. 9, peaks at 6 pole-pairs. The initial increase in thrust force for 3 to 6 pole-pairs is because the electrical frequency becomes greater, if operating at the same slip speed, as seen by (8), and thus the magnet flux density has more time available to penetrate further into the track and interact with the induced currents to create thrust force. The decreasing thrust force (above 6 pole-pairs) is a result of the magnitude of the magnetic flux density decreasing with the greater number of pole-pairs. Fig. 10 shows that the peak lift-to-weight ratio is achieved using 4 pole-pairs.

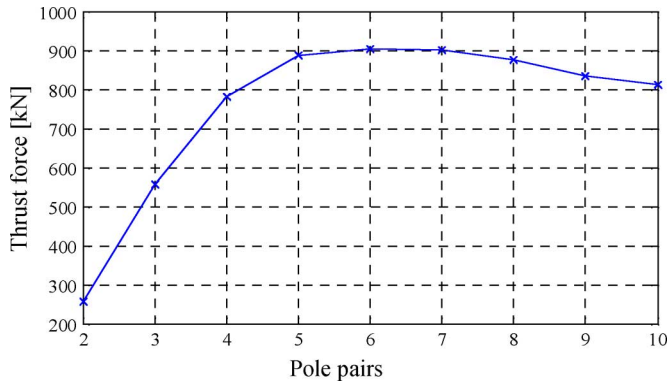

Fig. 9. Thrust force versus pole-pairs.

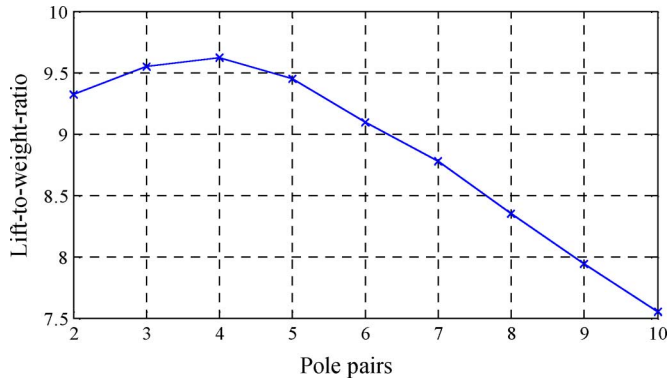

Fig. 10. Lift-to-weight ratio versus pole-pairs.

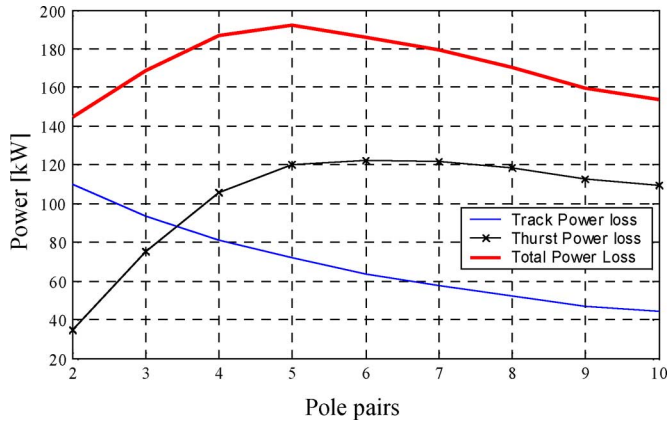

Fig. 11. Track and thrust power versus pole-pairs.

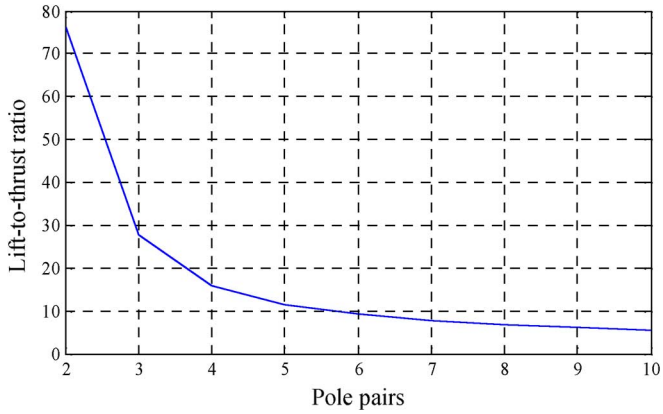

Fig. 12. Lift-to-thrust ratio versus pole-pairs.

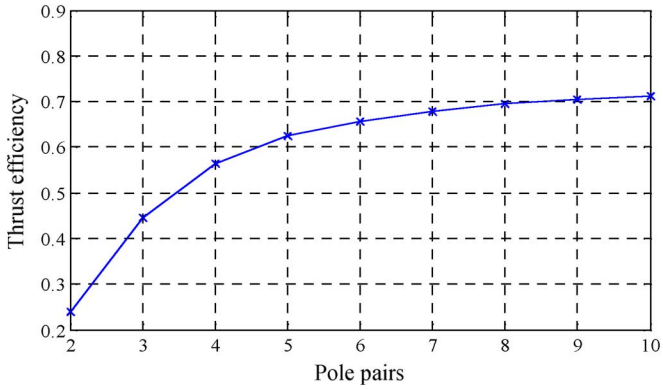

Fig. 13. Thrust efficiency versus pole-pairs.

TABLE III
SIMULATION PARAMETERS FOR POLE-PAIR ANALYSIS

Translational velocity, v_x	135ms^{-1}
Slip speed, s	45 ms^{-1}
Outer radius, r_o	0.23m
Track conductivity, σ	3.5×10^{7}Sm^{-1}
Track thickness, t	10mm
Magnet width, w	0.2m
Air gap, g	10mm
Pole pairs, P	varied

The combination of a decreasing thrust and lift force above 5 pole-pairs results in a decreasing total power use within the track, as illustrated in Fig. 11. But, since the lift force decreases at a faster rate than the thrust force, as shown in Fig. 12, the thrust efficiency continues to increase, as shown in Fig. 13. The improvement in thrust efficiency with increased pole-pairs is well known by SLIM designers and thus should be expected for the EDW [3]–[7].

Using a small number of pole-pairs gives the lowest watts-per-kilogram as shown in Fig. 14. However, for small pole-pair numbers, the track power loss is the largest and the level of thrust efficiency is the lowest. Therefore, if only lift force is required, the best strategy would be to make the watts-per-kilogram the smallest. But, since both lift and thrust are required for maglev applications, a direct tradeoff between the watts-per-kilogram,

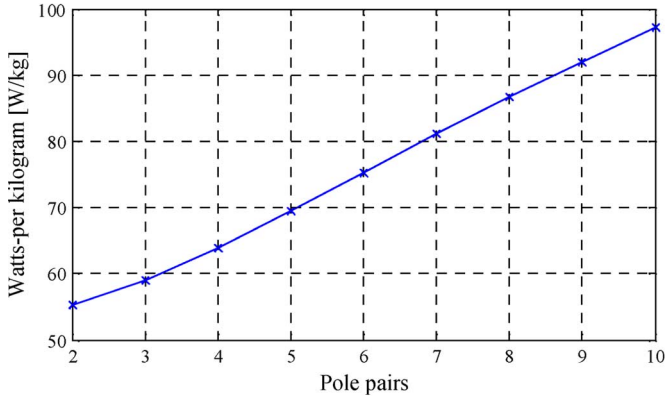

Fig. 14. Watts-per-kilogram for lift versus pole-pairs.

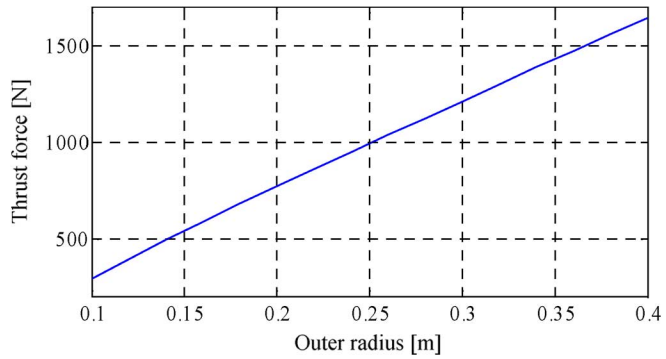

Fig. 15. Thrust force versus outer radius.

which represents the lift efficiency and the thrust efficiency performance metric is evident. This tradeoff clearly shows the interrelationship between the thrust and lift forces. One can obtain a higher thrust efficiency (higher thrust-per-watt) at the cost of a lower lift efficiency (higher watts-per-kilogram), or a higher lift efficiency (lower watts-per-kilogram) at the cost of a lower thrust efficiency (lower thrust-per-watt).

The pole-pair analysis shows that in order to create maximum thrust efficiency the highest number of pole-pairs should be chosen that still provides a sufficient lift-to-weight ratio. Thus, the ability to improve the thrust efficiency while still providing sufficient lift force is limited by the available rotor magnetic flux density.

B. Rotor Radius

The influence of the outer radius on the performance metrics is illustrated in Figs. 15–25. The parameters used in the analysis are shown in Table IV. Fig. 15 and Fig. 16 show that as the outer radius increases the lift and thrust forces increase linearly as the thrust and lift forces are basically proportional to the track surface area covered by the rotor. However, since the rotor magnet mass increases by the square of the radius, as shown in Fig. 17, the lift-to-weight-ratio decreases with increasing outer radius, as shown in Fig. 18 and Fig. 19. At very low radii the flux along the track at the chosen air-gap becomes very weak and this causes the reduction in the lift-to-weight ratio below 0.15 m. This reduction in the lift-to-weight ratio at small radii becomes severe

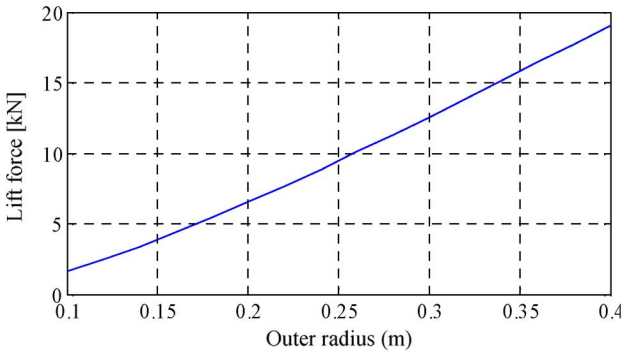

Fig. 16. Lift force versus outer radius.

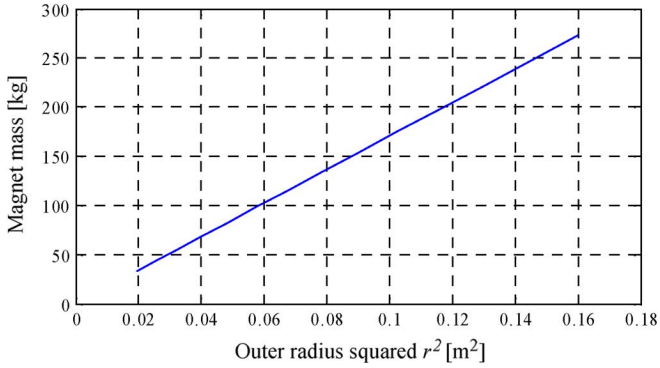

Fig. 17. Magnet mass versus outer radius squared.

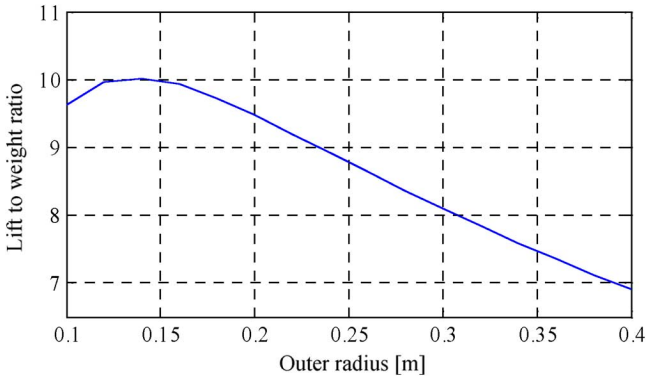

Fig. 18. Lift-to-weight ratio versus outer radius.

above 6 pole-pairs. Also, as the outer radius increases the lift force increases at a faster rate than the thrust force and this leads to an increasing lift-to-thrust ratio as shown in Figs. 20 and 21.

The increase in outer radius improves the thrust efficiency as shown in Figs. 22 and 23. For higher outer radii, the slip speed must be increased in order to be at the peak thrust efficiency. This is why Fig. 22 does not show the full benefit obtained by increasing the radii. The slip speed must be increased because as the outer radii increases the electrical frequency decreases when at the same circumferential velocity, ν_c, as shown by (7).

Lastly, Fig. 24 shows that the watts-per-kilogram decreases as the outer radius increases and this is because the lift force increases at a greater rate compared to the power dissipated in the track (Fig. 25).

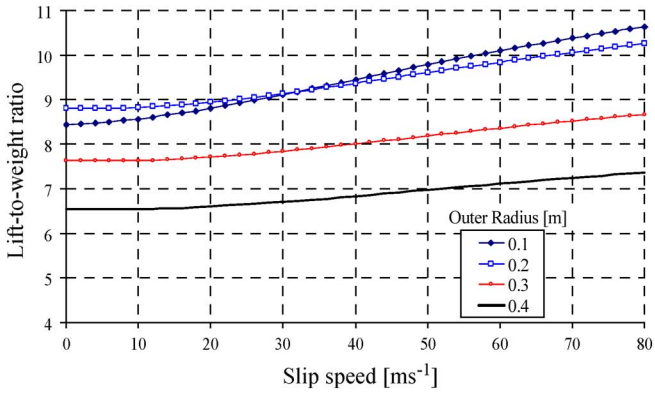

Fig. 19. Lift-to-weight ratio versus slip speed for a range of outer radii.

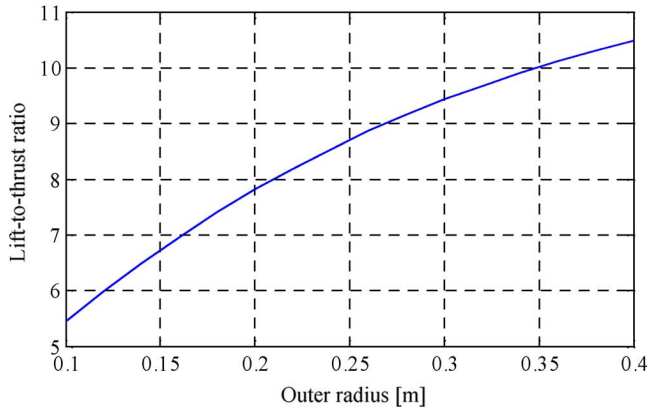

Fig. 20. Lift-to-thrust ratio versus outer radius.

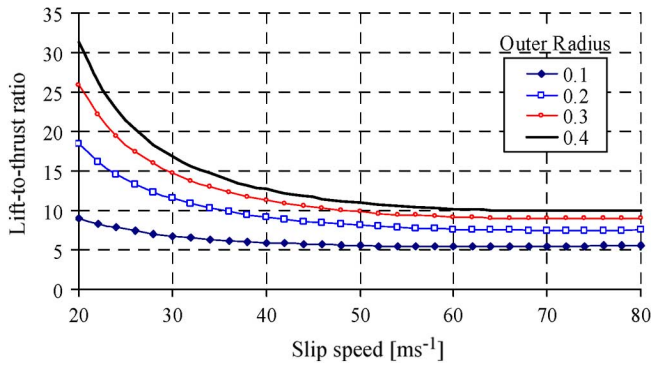

Fig. 21. Lift-to-thrust ratio versus slip speed for a range of outer radii.

C. Rotor Radius Versus Pole Pairs

If it is assumed that the optimal radius ratio is used, then the outer radius and number of pole-pairs are the only parameters that can vary on the rotor. Therefore, it should be instructive to see how interrelated these two parameters are. Plots of the lift-to-weight-ratio, thrust efficiency and lift-to-thrust ratio versus pole-pairs and outer radius are shown in Figs. 26–28. The parameters used to generate the plots are the same as given in Table III. As expected, the thrust efficiency increases with an increasing number of pole-pairs, but as the number of pole-pairs increases the outer radius has a diminishing effect on efficiency, at the fixed slip speed value. In contrast, both the outer radius

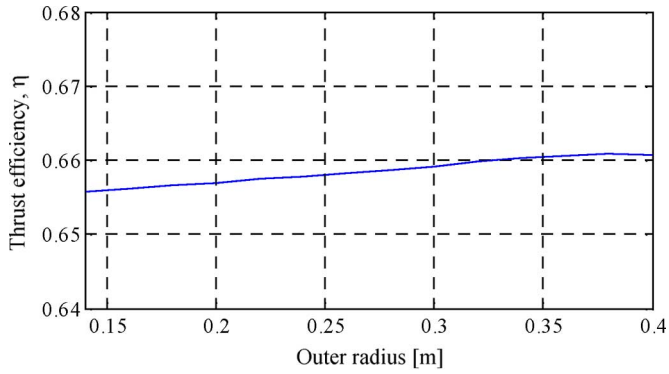

Fig. 22. Thrust efficiency versus outer radius.

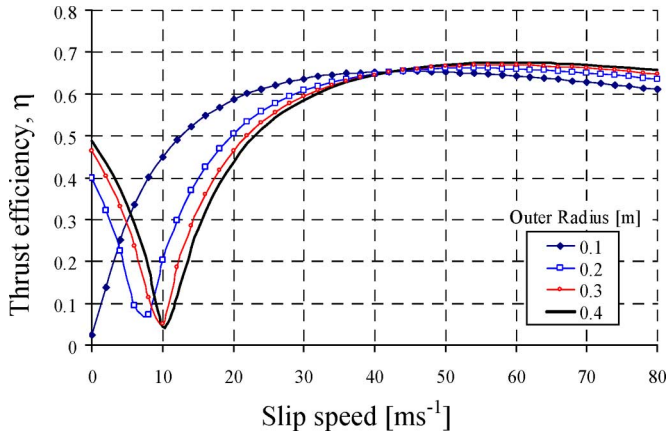

Fig. 23. Thrust efficiency versus slip speed for a range of outer radii.

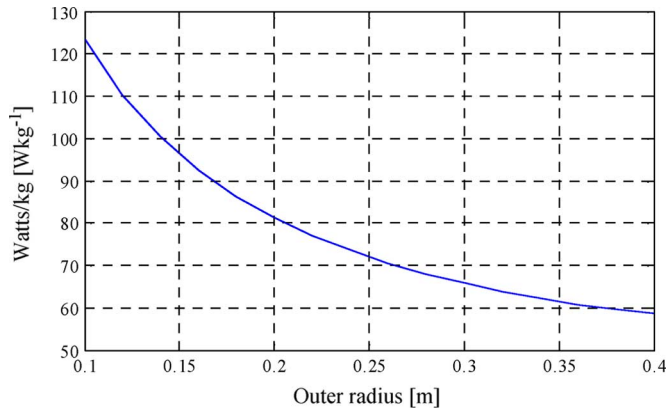

Fig. 24. Watts-per-kilogram versus outer radius.

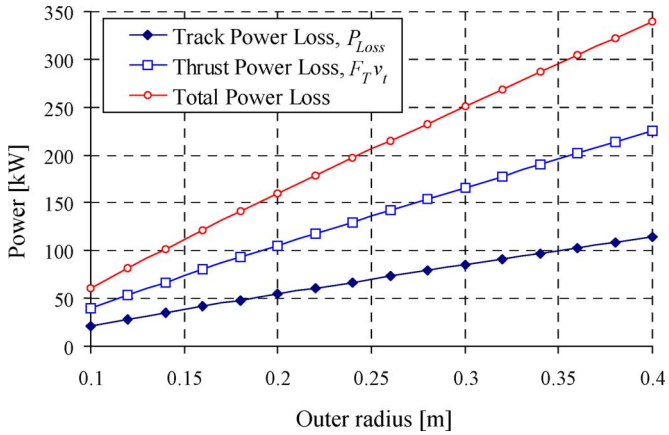

Fig. 25. Track power versus outer radius.

TABLE IV
PARAMETERS USED IN THE OUTER RADIUS ANALYSIS

Translational velocity, v_x	135ms^{-1}
Slip speed, s	45ms^{-1}
Outer radius, r_o	varied
Inner radius, r_i	0.79or
Pole pairs, P	6
Track conductivity, σ	3.5×10^{7}Sm^{-1}
Track thickness, t	10mm
Magnet width, w	0.2m
Air gap, g	10mm

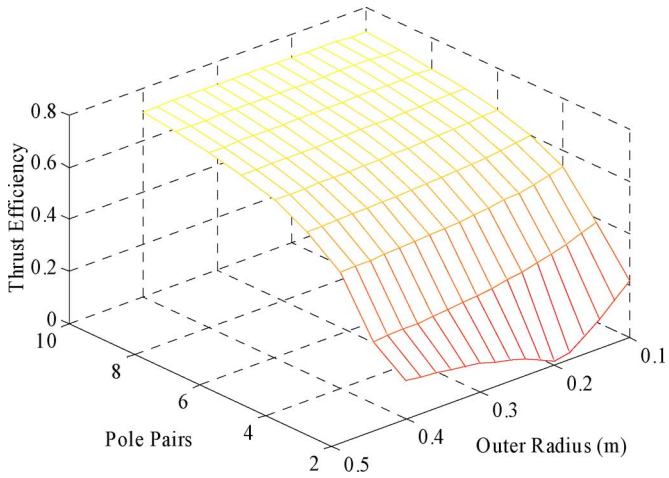

Fig. 26. Thrust efficiency versus outer radius and pole-pairs.

and pole-pairs significantly influence the lift-to-weight ratio, as shown in Fig. 27. Either using a higher number of pole-pairs or a higher outer radii will result in a diminished lift-to-weight ratio because of the reduction in field strength at the track surface.

Fig. 28 shows that using an increased number of pole-pairs decreases the lift-to-thrust ratio but increasing the outer radius improves the lift-to-thrust ratio performance. Thus, it can be concluded that the pole-pairs and outer radius should be made as large as possible so as to create the highest thrust efficiency and lift-to-thrust ratio combination. However, this increase is limited by the need to achieve a sufficient lift-to-weight ratio. This analysis has been used as a guide in designing the experimental model [40]. A summary of how the outer radius and pole-pairs affect the performance is shown in Table V.

D. Track Conductivity

An increase in conductivity decreases the thrust force while the lift force increases. This result is because as the conductivity increases larger currents flow within the track and therefore the currents prevent the vertical rotor magnet field from penetrating fully into the track.

The decrease in thrust and increase in lift with conductivity results in a decrease in thrust efficiency, but an increase in the lift-to-weight ratio. Thus, a higher conductive track, such

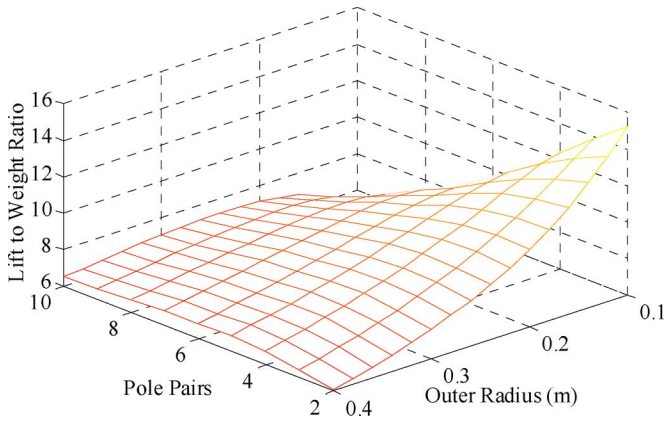

Fig. 27. Lift to weight ratio versus pole-pairs and outer radius.

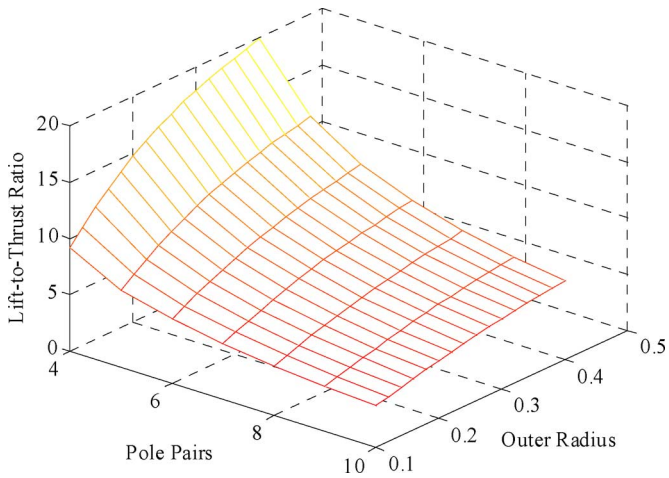

Fig. 28. Lift-to-thrust ratio versus pole-pairs and outer radius.

TABLE V
TRADEOFFS BETWEEN OUTER RADIUS AND POLE PAIRS

	Increase in Pole-Pairs	Increase in Outer Radius
Efficiency, η	↑	↑
Lift-to-thrust ratio, F_l/F_T	↓	↑
Lift-to-weight ratio, L_w	↓	↓

TABLE VI
PARAMETERS USED FOR THE TWO EDW COMPARISONS

Translational velocity	135 ms^{-1}
Slip speed	varied
Outer radius	0.23m
Pole pairs	6
Guideway thickness	10 mm
Magnet width	0.2 m
Air gap	10 mm
Rotor separation	0.175 m
Guideway conductivity	$3.5\times10^{7}Sm^{-1}$

as copper, could be used to improve the lift-to-weight performance, but the thrust efficiency would decrease. However, with a higher lift-to-weight ratio a higher pole-pair number can be used and this would then increase the efficiency, but decrease the lift force. The result would be similar performance

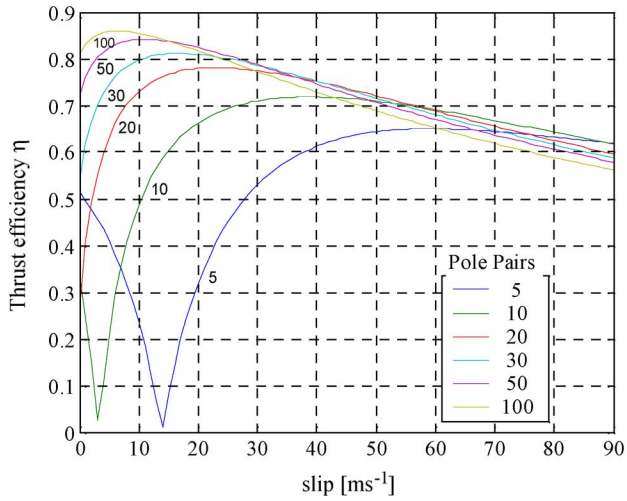

Fig. 29. Thrust efficiency versus slip when using a high number of poles.

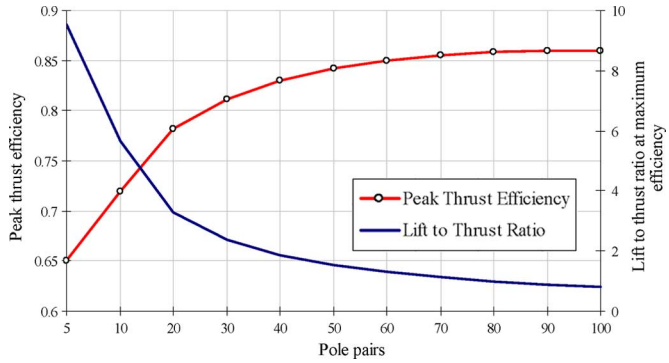

Fig. 30. Peak thrust efficiency and corresponding lift-to-thrust ratio when using a high number of poles.

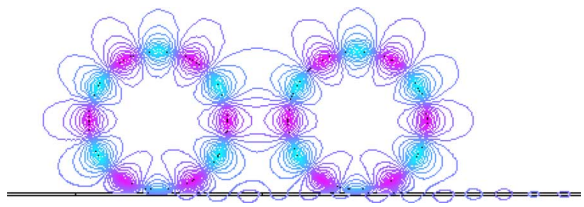

Fig. 31. Two EDWs in series separated by 0.175 m.

to aluminum but at a higher cost, therefore aluminum appears to be the most cost effective material to use.

E. Track Thickness

Increasing the track thickness only has an effect on the forces when the magnetic diffusion depth is larger than the track thickness. Therefore, reducing the track thickness below the skin-depth increases the track resistance and predictably increases the thrust and decreased the lift force. A track thickness greater than 10 mm would likely not be necessary because at high-speed the skin depth is at or below this level.

V. IMPROVING ELECTRODYNAMIC WHEEL PERFORMANCE

There are a number of ways in which the thrust efficiency could be improved further. If higher B_r magnet material could

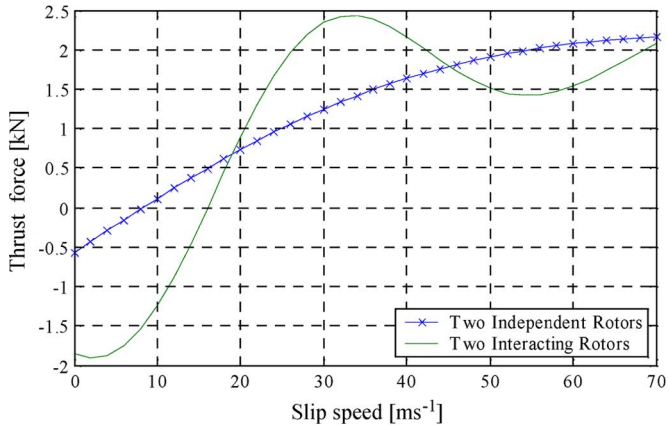

Fig. 32. Thrust force comparison.

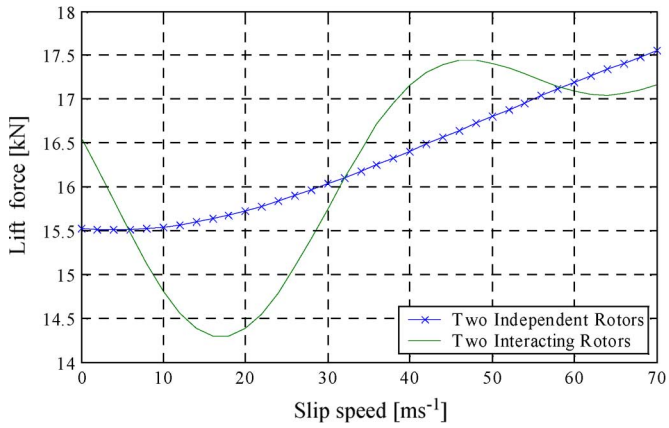

Fig. 33. Lift force comparison.

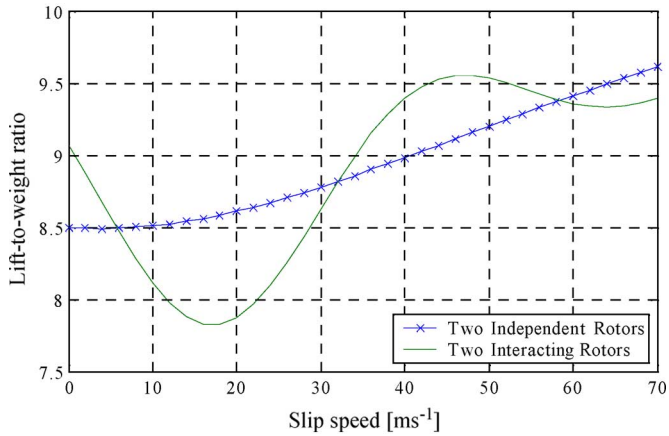

Fig. 34. Lift-to-weight ratio comparison.

be used, or if superconducting magnets were used, then the thrust efficiency could be improved further by increasing the number of poles while still providing a sufficient lift-to-weight ratio. For instance, using the parameters given in Table VI the results for increasing the number of poles well beyond 10 pole-pairs is shown in Fig. 29; at 100 pole-pairs the thrust efficiency reaches 87%. With such a high pole number the magnitude of the lift force becomes less than the thrust force

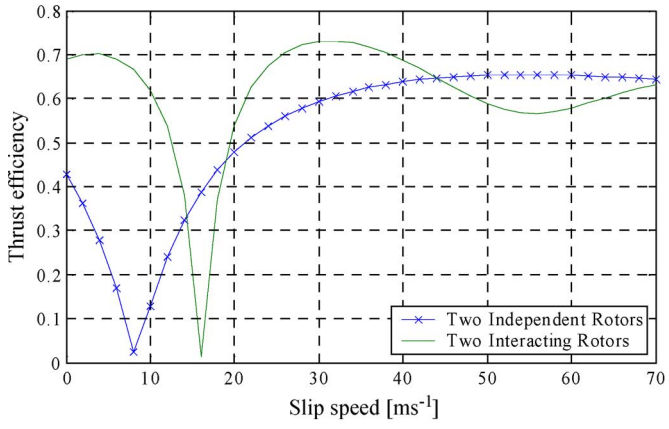

Fig. 35. Thrust efficiency comparison.

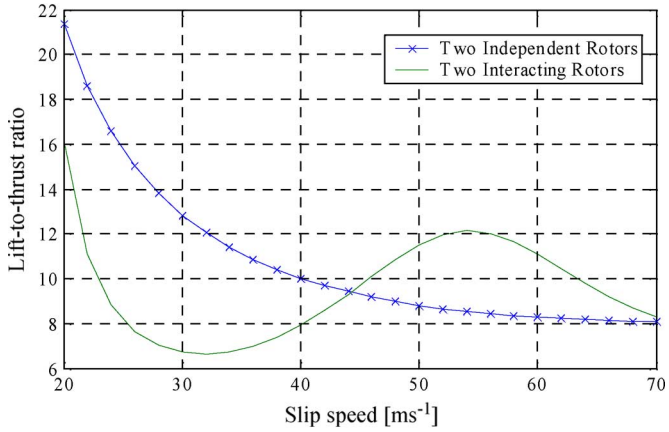

Fig. 36. Lift-to-thrust ratio comparison.

TABLE VII
IMPROVEMENT IN PERFORMANCE WHEN USING TWO ELECTRODYNAMIC WHEELS IN SERIES (AT PEAK THRUST EFFICIENCY)

Parameter	Two Independent Rotors	Two Interacting Rotors	% Change
Slip speed [ms^{-1}]	54	32	-41
Lift force, F_L [kN]	17.0	16.1	-5
Lift-to-weight ratio	9.29	8.81	-5
Thrust force, F_T [kN]	1.99	2.43	+22
Lift-to-thrust ratio, F_L/F_T	8.54	6.64	-22
Track power loss, P_{Loss} [kW]	141.5	121.0	-14
Total power requirement [kW]	410	448	+9
Thrust efficiency	0.66	0.73	+11

as shown in Fig. 30 and therefore only when operating with a very high thrust force would sufficient lift force be created to enable suspension.

A second method to improve performance is to use more than one EDW in series, and this would almost certainly be required for any large vehicle. An illustration of a simulation with two EDW in series is shown in Fig. 31. If the second EDW is close to the first then the currents induced in the track by the first EDW can be used by the second, and thus less overall energy is required.

The effect of using the two EDWs in series was compared with the performance achievable by using two EDWs that are

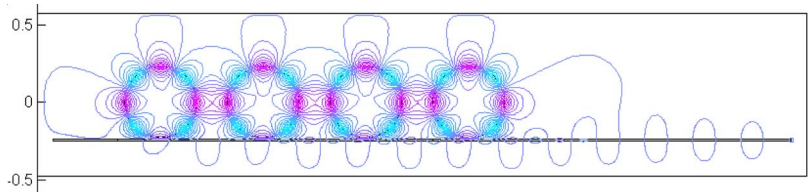

Fig. 37. Magnetic field contour plot for four electrodynamic wheels in series.

TABLE VIII
PEAK THRUST EFFICIENCY FOR DIFFERENT POLE-PAIRS AND WHEEL NUMBERS AT 135 ms^{-1} TRANSLATIONAL VELOCITY

EDW's in Series	**1**		**2**			**3**			**4**			**5**		
Pole-Pairs	η_p	s	η_p	*Sep.*	s	η_p	*Sep.*	s	η_p	*Sep.*	s	η_p	*Sep.*	s
3	0.57	92	0.70	0.325	50	0.76	0.35	40	0.79	0.35	36	0.81	0.375	30
4	0.61	80	0.72	0.175	38	0.78	0.175	32	0.81	0.175	28	0.83	0.200	22
5	0.64	66	0.72	0.250	42	0.77	0.125	10	0.80	0.125	8	0.80	0.300	26
6	0.66	54	0.73	0.175	32	0.77	0.175	28	0.79	0.175	26	0.81	0.200	20
7	0.67	54	0.72	0.250	32	0.77	0.125	16	0.78	0.250	28	0.78	0.250	28

not interacting, either because they have a large separation distance, or are on different tracks. The results from the comparison are shown in Figs. 32–36. The parameters used to make the comparison are shown in Table VI. The figures show that with the additional rotor interacting, the slip speed needs to be larger before the thrust becomes positive. However, a significantly higher maximum thrust is achievable, and this results in higher thrust efficiency. In addition, a higher lift force can also be achieved, which results in a larger lift-to-weight ratio. The results show that there is a range of slip speed values where both the lift-to-weight ratio and thrust efficiency are higher than if the two EDWs were not interacting. A summary of the improvements in performance is shown in Table VII. The percentage changes that improve performance have been shaded.

Encouraged by the potential improvements obtained by using 2 EDWs in series, a study of the effect of using up to 5 EDWs in series was undertaken. The parameters used in the simulation are the same as given in Table VI, but the separation distance between rotors, Sep, and pole-pairs, P, were also varied. The phase difference between the rotors was kept constant. A lift-to-weight ratio of 8 or greater was always ensured. An example showing the field lines created by 4 EDWs in series is shown in Fig. 37. A summary of the simulation results is given in Table VIII. The peak thrust efficiency, η_p, and corresponding slip speed, s, is also shown. Rotor separation distances less than 0.125 m were not considered because this created too large a field between the rotors. However, since an arch motor over the top of each EDW is expected to be used to rotate the EDWs, a lower separation distance may be achievable (such as 0.1 m) enabling somewhat higher operating thrust efficiencies than shown. As the number of series EDWs increases the peak efficiency occurs at a lower pole-pair value. As for the SLIM, the thrust efficiency improves with length [3], [5], but even with 5 EDWs in series the design should be much shorter than for a high-speed SLIM [3].

VI. CONCLUSION

A 2-D steady-state model has been used to investigate the parameters that affect the performance of an electrodynamic wheel. Tradeoffs between the lift and thrust performance have been highlighted. It was shown that using multiple electrodynamic wheels in series can improve the performance of such an integrated maglev device. Although additional losses will occur due to requiring motors for rotation of the electrodynamic wheel, it will not suffer from a low power factor. The lift and thrust forces can be generated by using just one mechanism and the same track surface.

ACKNOWLEDGMENT

The authors would like to acknowledge the support provided by the member companies of the Wisconsin Electric Machines and Power Electronics Consortium (WEMPEC) at the University of Wisconsin-Madison. Also, the authors would gratefully like to thank the Magsoft Corporation for the use of their finite element analysis software.

REFERENCES

[1] J. H. Dannan *et al.*, "A linear induction motor propulsion system for high-speed ground vehicles," *Proc. IEEE*, vol. 61, no. 5, pp. 621–630, May 1973.
[2] J. F. Eastham *et al.*, "Comparison of short primary linear machines for high speed maglev vehicles," *IEEE Trans. Magn.*, vol. MAG-23, no. 5, pp. 2338–2343, Sep. 1987.
[3] S. Nonaka and T. Higuchi, "Design strategies of single-sided linear induction motors for propulsion of vehicles," in *Int. Conf. Maglev and Linear Drives*, Las Vegas, NV, 1987, pp. 1–5.
[4] M. Iwamoto *et al.*, "End-effect of high-speed linear induction motor," *IEEE Trans. Ind. Appl.*, vol. IA-9, no. 6, pp. 632–638, Nov. 1973.
[5] S. Yamamura, *Theory of Linear Induction Motors*. Tokyo, Japan: Univ. Tokyo Press, 1979, pp. 3–123.
[6] M. Iwamoto and S. Yamamura, "End effect of high-speed linear induction motors," *Electr. Eng. Jpn.*, vol. 92, pp. 94–101, Jun. 1972.
[7] V. E. Skobelev, "The problems of using the asynchronous linear motor for high-speed ground transport," *Rail Inter.*, pp. 297–308, June 1977.
[8] T. R. Haller and W. R. Mischler, "A comparison of linear induction and linear synchronous motors for high speed ground transportation," *IEEE Trans. Magn.*, vol. MAG-14, no. 5, pp. 924–926, Sep. 1978.
[9] G. B. Kliman, "Linear electric motors," in *IEEE Ind. Appl. Conf.*, 1980, pp. 256–261.
[10] G. B. Kliman *et al.*, "Experimental evaluation of a high speed double sided linear induction motor," *IEEE Trans. Power App. Syst.*, vol. PAS-94, no. 1, pp. 10–17, Jan. 1975.
[11] T. A. Lipo and T. A. Nodahl, "Pole-by-pole d-q model of a linear induction machine," *IEEE Trans. Power App. Syst.*, vol. 98, no. 2, pp. 629–639, Mar./Apr. 1979.

[12] M. Iwamoto *et al.*, "Experimental and theoretical study of high-speed single-sided linear induction motors," *IEE Proc. B*, vol. 128, pp. 306–312, Nov. 1981.
[13] J. J. Stickler, "Comparison of theories for high-speed linear induction motors," *IEEE Trans. Veh. Technol*, vol. 29, pp. 65–71, Feb. 1980.
[14] E. R. Laithwaite, "Application of linear induction motors to high-speed transport system," *Proc. IEE*, vol. 116, pp. 713–724, 1969.
[15] K. Chirgwin, "Linear electric motor propulsion systems," in *Transport Without Wheels*, E. R. Laithwaite, Ed. London, U.K.: Elek Books Ltd, 1977, pp. 37–59.
[16] R. H. Borcherts and L. C. Davis, "Lift and drag forces for the attractive electromagnetic suspension systems," *IEEE Trans. Magn.*, vol. 10, no. 3, pp. 425–428, Sep. 1974.
[17] S. Yamamura and T. Ito, "Analysis of speed characteristics of attracting magnet for magnetic levitation of vehicles," *IEEE Trans. Magn.*, vol. MAG-11, no. 5, pp. 1504–1507, Sep. 1975.
[18] G. H. Bohn *et al.*, "A contribution to magnetic levitation technology," in *Proc. Fourth Int. Cryo. Eng. Conf.*, Eindhoven, The Netherlands, 1972, pp. 202–208.
[19] G. H. Bohn, "The influence of eddy currents on an electromagnetic levitation system," in *2nd Conf. Advances in Magnetic Materials and Their Appl.*, London, U.K., 1976, pp. 104–107.
[20] J. F. Eastham and E. R. Laithwaite, "Linear induction motors as 'electromagnetic rivers'," *Proc. IEE*, vol. 121, no. 10, pp. 1099–1108, Oct. 1974.
[21] J. F. Eastham and D. Rodger, "The performance of induction levitators," *IEEE Trans. Magn.*, vol. MAG-20, no. 5, pp. 1684–1686, Sep. 1984.
[22] R. M. Katz *et al.*, "Integrated magnetic suspension and propulsion of guided ground transportation vehicles with a SLIM," *IEEE Trans. Magn.*, vol. 15, no. 6, pp. 1437–1439, Nov. 1979.
[23] R. H. Borcherts and L. C. Davis, "The superconducting paddle-wheel as an integrated propulsion levitation machine for high speed ground transportation," *Electr. Mach. Electrom.*, vol. 3, pp. 341–355, Apr.–June 1979.
[24] L. C. Davis and R. H. Borcherts, "Superconducting paddle wheels, screws, and other propulsion units for high-speed ground transportation," *J. Appl. Phys.*, vol. 44, pp. 3294–3299, Jul. 1973.
[25] M. Kawai and H. Ariga, "Equos-LIM-CAR," (in Japanese) *The Invention*, vol. 89, pp. 70–77, 1992.
[26] N. Fujii *et al.*, "Three dimensional force of magnet wheel with revolving permanent magnets," *IEEE Trans. Magn.*, vol. 33, no. 5, pp. 4221–4223, Sep. 1997.
[27] N. Fujii *et al.*, "Characteristics of magnetic lift, propulsion and guidance by using magnet wheels with rotating permanent magnets," in *IEEE Ind. Appl. Conf.*, 2000, pp. 257–262.
[28] N. Fujii *et al.*, "Basic characteristics of magnet wheels with rotating permanent magnets," in *IEEE Ind. Appl. Conf.*, 1994, pp. 203–209.
[29] N. Fujii *et al.*, "Revolving magnet wheels with permanent magnets," *Electr. Eng. Jpn.*, vol. 116, pp. 106–117, 1996.
[30] I. Boldea and S. A. Nasar, *Linear Motion Electromagnetic Systems*. New York: Wiley, 1985, pp. 461–478.
[31] Philco-Ford, "Department of Transportation, Conceptual Design and Analysis of the Tracked Magnetically Levitated Vehicle Technology Program (TMLV)—Repulse Scheme Volume 1—Technical Studies," Department of Transport, Springfield, VA, Tech. Rep. DOT-FR-40024 (Task I), Feb. 1975.
[32] J. Bird and T. A. Lipo, "An electrodynamic wheel: An integrated propulsion and levitation machine," in *IEEE Int. Elect. Mach. Drives Conf.*, 2003, pp. 1410–1416.
[33] N. Fujii, Y. Ito, and T. Yoshihara, "Characteristics of a moving magnet rotator over a conducting plate," *IEEE Trans. Magn.*, vol. 41, no. 10, pp. 3811–3813, Oct. 2005.
[34] J. Bird and T. A. Lipo, "Calculating the forces created by an electrodynamic wheel using a 2D steady-state finite element model," *IEEE Trans. Magn.*, 2006, submitted for publication.
[35] J. Bird and T. A. Lipo, "The experimental verification of lift, thrust and guidance forces for an electrodynamic wheel rotating over a split-sheet guideway," in *19th Int. Conf. Magnetically Levitated Systems and Linear Drives*, Dresden, Germany, Sep. 2006.
[36] K. Halbach, "Design of permanent multipole magnets with oriented rare earth cobalt material," *Nucl. Instr. Meth.*, vol. 187, pp. 1–10, 1980.
[37] S.-M. Jang, S.-H. Lee, and S.-S. Jeong, "Characteristic analysis of eddy-current brake system using the linear Halbach array," *IEEE Trans. Magn.*, vol. 38, no. 5, pp. 2994–2996, Sep. 2002.
[38] Q. Han, C. Ham, and R. Phillips, "Four- and eight-piece Halbach array analysis and geometry optimisation for maglev," *IEE Proc. Elect. Power Appl.*, vol. 152, no. 3, pp. 535–542, May 2005.
[39] K. R. Davey, "Optimization shows Halbach arrays to be non-ideal for induction devices," *IEEE Trans. Magn.*, vol. 36, no. 4, pp. 1035–1038, Jul. 2000.
[40] J. Bird and T. A. Lipo, "A 3D magnetic charge finite element model of an electrodynamic wheel," *IEEE Trans. Magn.*, 2007, submitted for publication.

Manuscript received August 28, 2006; revised April 16, 2007. Corresponding author: J. Bird (e-mail: jbird@wisc.edu).